Nuclear Science and Techniques (2023) 34:159
https://doi.org/10.1007/s41365-023-01319-8

Two annular CsI(Tl) detector arrays for the charged particle telescopes

Hong-Yu Zhu[1] · Jian-Ling Lou[1] · Yan-Lin Ye[1] · Li-Sheng Yang[1] · Bo-Long Xia[1] · Kang Wei[1] · Ying Chen[1] · Wei-Liang Pu[1] · Zi-Yao Hu[1] · Hao-Yu Ge[1] · Jia-Hao Chen[1] · Kai Ma[1] · Wen-Wu Wan[1] · Hooi-Jin Ong[2] · Yan-Yun Yang[2] · Shi-Wei Xu[2] · Kang Wang[2] · Fang-Fang Duan[2] · Jun-Bin Ma[2] · Zhen Bai[2] · Peng Ma[2] · Ruo-Fu Chen[2]

Received: 27 April 2023 / Revised: 30 June 2023 / Accepted: 10 July 2023 / Published online: 31 October 2023

Abstract
In this study, we constructed two annular detector arrays comprising 24 wedge-shaped CsI(Tl) crystals, and tested them using an α source and radioactive beams of $^{14-16}$C on a CD_2 target. We compared the properties of a CsI(Tl) crystal encapsulated with various reflectors, revealing that using the 80-μm-thick ESR film to pack the CsI(Tl) crystal yielded the largest light output with the smallest non-uniformity in light output (ΔLO). For the 24 CsI(Tl) detectors with the 80-μm-thick ESR films, the average energy resolution improved as the average light output increased; however, it deteriorated as the ΔLO value increased. To form two annular Si-CsI(Tl) telescopes for identifying the light-charged particles, the ΔLO value and energy resolution of each CsI(Tl) detector were maintained under 20% and 7.7%, respectively. These telescopes were tested for the first time in a direct nuclear reaction experiment using $^{14-16}\mathrm{C} + d$. The results demonstrated that the $Z = 1$ and $Z = 2$ charged particles were adequately discriminated by the telescopes using the standard ΔE-E method.

Keywords Wedge-shaped CsI(Tl) detector · Light output non-uniformity · Si-CsI(Tl) telescope · Particle identification

1 Introduction

Thallium-activated cesium iodide (CsI(Tl)) detectors have been widely applied in nuclear and particle physics experiments owing to their several advantages. Primarily, CsI(Tl) is noted for its malleability and softness, which allows it to be manufactured into several irregular shapes, as required by physical experimental conditions at a relatively low cost. In addition, CsI(Tl) is not hygroscopic, which facilitates its storage. Furthermore, it can deliver a considerable stopping power owing to its high density ($\rho \approx 4.5$ g/cm^3). Therefore, it is commonly used to collect the residual energies of charged particles after punching through silicon (Si) strip detectors. Combining Si-CsI(Tl) forms an effective approach for identifying charged particles using the telescope technique with the standard ΔE-E method. LASSA [1], MUST2 [2], FARCOS [3, 4], and HiRA [5–7] are examples of such combinations. A similar detection array is displayed in Fig. 1, dedicated to the kinematically complete measurement of charged particles produced from the direct nuclear reactions of radioactive ion beams with a CH_2 or CD_2 target. This was developed at Peking University [8–10].

As depicted in Fig. 1, the array comprised several telescopes. To measure the projectile-like particles, telescope T0 was installed at approximately 0° relative to the secondary beam direction, while T1 was placed close to 90° to detect the recoil protons or deuterons from the elastic or inelastic scattering of the radioactive beams on the CH_2 or CD_2 targets. A set of annular telescopes, referred to as TA-upstream, is positioned upstream of the physical target to detect the protons produced from the (d, p) reaction [11–13]. Another set of annular telescopes, called TA-downstream, is installed downstream to identify ^{3}He/^{4}He, p, d, and t from the (d, ^{3}He/^{4}He), (p, p'), (p, d)(or (d, d')),

This work was supported by the National Natural Science Foundation of China (Nos.12275007, U1867214, 11775004), the funding from the State Key Laboratory of Nuclear Physics and Technology, Peking University, China (No. NPT2021ZZ01) and funding from heavy Ion Research Facility, Lanzhou, China (No. HIR2021PY002).

✉ Jian-Ling Lou
jllou@pku.edu.cn

1 School of Physics and State Key Laboratory of Nuclear Physics and Technology, Peking University, Beijing 100871, China

2 Institute of Modern Physics, Chinese Academy Sciences, Lanzhou 730000, China

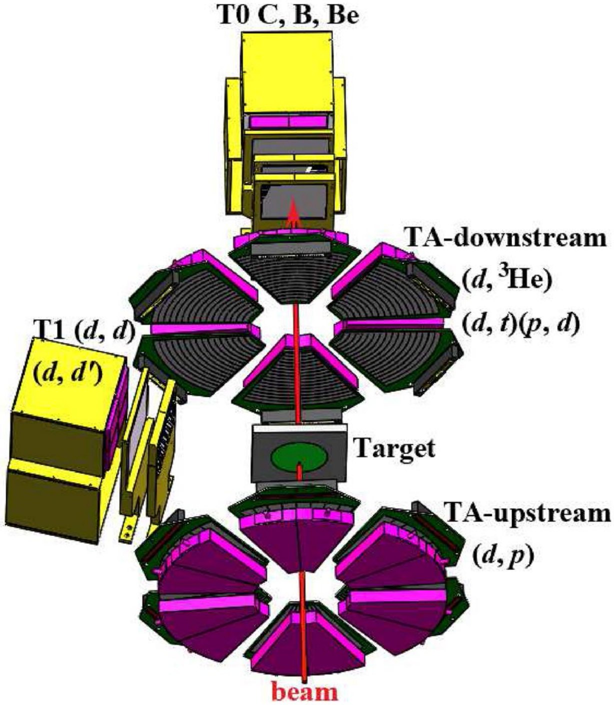

Fig. 1 (Color online) Schematic of the detection array developed at Peking University, which is designed to detect charged particles produced from direct reactions induced by a radioactive beam impinging on a CH_2 and CD_2 target. Two sets of annular telescopes named TA-upstream and TA-downstream are installed upstream and downstream of the physical target, respectively, to detect light-charged particles from different reaction channels

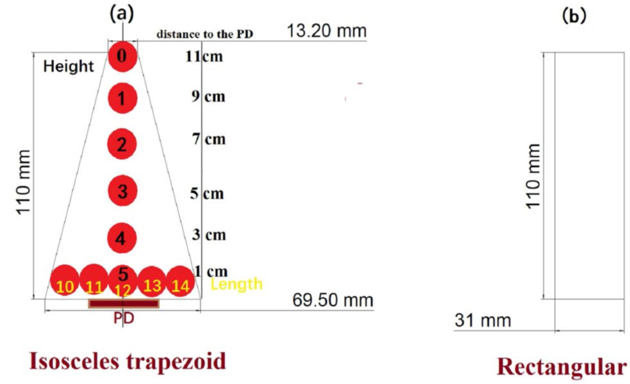

Fig. 2 (Color online) **a** Front and **b** side view of a CsI(Tl) detector. Scan positions along its height and length are labeled as black and yellow numbers, respectively. In (a), the red-solid circles represent collimators with a diameter of 12 mm, while the dark-brown rectangular at the bottom of the isosceles trapezoid represents the PD. Center of collimators 0 through 5 were at an approximate distance of 11, 9, 7, 5, 3, and 1 cm from the PD, respectively. Vertical distance between the center of each collimator along the longer side of the isosceles trapezoid and the PD is identical (1 cm)

and (p, t) (or (d, t)) reactions, respectively [10, 14–20]. The TA-upstream and TA-downstream have similar structures, comprising six annular double-sided silicon strip detectors (DSSDs) and 12 wedge-shaped CsI(Tl) detectors. For the DSSDs, two distinct thicknesses, namely, 150 and 400 µm, were selected. Each DSSD was segmented into 6.4-mm-width rings on one side directed to the physical target and into eight fan-shaped regions on the other side. The inner and outer radii of the TA-upstream were set at 3.25 and 13.5 cm, respectively, to encompass the angles ranging from 135 to 165 ° in a laboratory frame for a typical (d, p) experiment [12, 13]. The inner radius and the covered angular span of the TA-downstream, which closely surrounds T0, can be readily adjusted based on variations in T0 for various experimental purposes. For instance, let us consider the ^{15}C(d, ^{3}He) experiment [16]: the inner radius of the TA-downstream was 6.0 cm, and it covered angles from 25 to 55 ° in the laboratory frame. Two CsI(Tl) detector arrays were positioned behind the DSSDs in the TA-upstream and TA-downstream, to form two annular Si-CsI(Tl) telescopes.

In this study, we focus on the construction and investigation of the properties of two annular CsI(Tl) detector arrays. The experimental details and results of the CsI(Tl) detector are described in Sect. 2. The properties of the two annular arrays, including the light output and nonuniformity, are discussed in Sect. 3. The particle identification (PID) spectra of the annular Si–CsI(Tl) telescopes measured in a direct nuclear reaction experiment of $^{14-16}$C + d are presented in Sect. 4. Finally, a brief summary is provided in the last section.

2 Details and experimental results of one wedge-shaped CsI(Tl) detector

2.1 Details of one wedge-shaped CsI(Tl) detector

Two CsI(Tl) detectors were assembled into a single unit and positioned behind a unit of annular DSSD to form a typical ΔE-E telescope. The geometric size and the photodiode (PD) position (dark-brown rectangle) of the CsI(Tl) detector are illustrated in Fig. 2. This crystal shape was selected owing to its superior properties observed in Geant4 simulations as well as the experimental results with an α source and a radioactive beam of ^{15}C [16]. However, the nonuniformity in light output of this long-tapered CsI(Tl) crystal decreased the energy resolution of the crystals and further affected the particle identification (PID) capability of the $\Delta E - E$ method, which was regarded as nonnegligible. In addition, the detection thresholds for the $Z = 1$ and $Z = 2$ isotopes were observed to be slightly higher, probably because of the low light output of the CsI(Tl) crystal, as well as the low sensitivity and large electronic noise of the preamplifier.

Thus, these properties should be improved before constructing CsI(Tl) detector arrays.

As illustrated in Fig. 2, the entrance and exit surfaces of the charged particles were the same isosceles trapezoid with the longer side tapering from 69.5 to 13.2 mm, while the four peripheral surfaces were rectangular. Each CsI(Tl) exhibited a height of 110 mm, which was slightly greater than the radius of the annular DSSD to prevent oblique penetration of the CsI(Tl) crystal by charged particles incident on the DSSD edge. The thickness of each crystal was designed to be 31 mm, which was adequate for ceasing the protons with energies up to 80 MeV. All surfaces of each crystal were polished nominally. The entrance surface directed toward the DSSD was covered with a 2-μm-thick aluminized Mylar film to facilitate the passage of charged particles and partially prevent the leakage of the scintillation light from the crystals. All other surfaces were encapsulated with reflectors to reflect the scintillation light back into the crystals. The scintillation light propagated within the crystal and was reflected on the reflectors several times until it was collected by the readout device.

Because of their low operational voltage, compact volume, insensitivity to magnetic fields, and adequate optical response with CsI(Tl), PDs and SiPMs are usually used for readouts [21]. In this study, a PD with an active area of 28 × 28 mm (S3584-08, Hamamatsu Photonics) [22] was selected as the photon-detection device for the CsI(Tl) crystal owing to its larger active area and lower temperature dependence. The PD was coupled to the CsI(Tl) readout surface using optical silicone grease.

2.2 Experimental results

A CsI(Tl) detector was initially tested using an ^{241}Am source that emitted α particles with an energy of 5.486 MeV and an absolute intensity of 85.2%. The source was collimated by a circular hole with a diameter of 1.2 cm and placed approximately 1.0 cm from the entrance surface; the source and collimation holes exhibited a similar size. As depicted in Fig. 2, six and five points were scanned with an equal interval of 2.0 and 1.2 cm along the height and length of the CsI(Tl) crystal, respectively, to measure the light output nonuniformity. In Fig. 2, the collimators are depicted as red circles and the scan positions are labeled with black and yellow numbers denoting their height and length, respectively. The center of each position (0, 1, 2, 3, 4, and 5) was approximately 11, 9, 7, 5, 3, and 1 cm away from the PD, respectively, and the vertical distance between the center of the positions (11, 12, 13, 14, and 15) along the longer side of the crystal and the PD was identical (1 cm). The scan position labeled 5 (black number) corresponds to that labeled 12 (yellow number).

A charge-sensitive preamplifier with an adjustable sensitivity was used to acquire the electronic signals produced by the PD. A shaping amplifier (ORTEC 572A) [23] closely followed the preamplifier. The unipolar signal from the amplifier was subsequently inputted into a Multichannel Analyzer (MCA). A voltage supplier, preamplifier, amplifier, and MCA were installed outside the vacuum chamber. To reduce the electronic noise, the cables connecting the PD, flange, and preamplifier were shielded with a weaving copper mesh and maintained as short as possible. To increase the signal amplitude and decrease the threshold of the CsI(Tl) detector, the sensitivity of the preamplifier was adjusted to approximately 6 mV/MeV for the α particles.

The typical energy spectrum measured at scan position 2 is illustrated in Fig. 3. The spectrum was fitted with only one Gaussian peak, indicated by the solid red curve in Fig. 3. The peak was asymmetric, primarily because of the low-energy α particles (5.443 MeV) emitted from the ^{241}Am source with a relatively small intensity (12.8%). The asymmetry of this peak could also be attributed to fewer unknown wrinkles on the Mylar film, although we attempted our best to smoothen these wrinkles. The centroid of the fitted Gaussian peak was proportional to the light output.

Energy resolution was determined by evaluating the ratio of full width at half maximum (FWHM) to the centroid of the fitted Gaussian peak. To enhance the properties of the CsI(Tl) detector, we attempted to enhance the light output and reduce the energy resolution, i.e., to increase the centroid and decrease the FWHM of the Gaussian peak under the same test conditions.

As reported in Ref. [16], the amount of light output and its nonuniformity rely on the intrinsic properties (e.g., Tl doping level), surface roughness (polished or rough), geometric shape (tapering angle), PD size, reflector (wrapping materials), and optical coupling materials of the CsI(Tl) detector. In this study, 24 polished CsI(Tl) crystals with identical shapes (Fig. 2) and a definitive amount of Tl

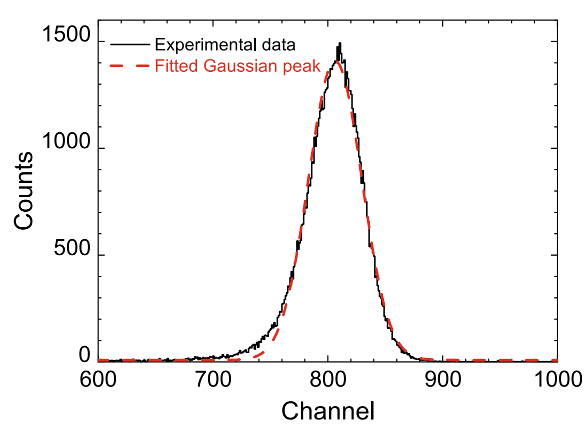

Fig. 3 Typical energy spectrum measured by one CsI(Tl) detector using an ^{241}Am source, which was positioned at scan position 2 with the collimator

doping were produced by the Institute of Modern Physics. To improve the performance of detectors, only the reflectors or PDs can be altered during fabrication.

Based on our experience with cubic CsI(Tl) detectors, we initially selected Tyvek paper as the reflector [24] in an experiment with a radioactive beam of ^{15}C [16]. Tyvek paper is neither purely specular nor diffuse. An enhanced specular reflector (ESR) film [25], which is the latest reflector used for CsI(Tl) scintillators, is mostly a specular reflector [26, 27]. According to the simulation results for the CsI(Tl) crystal displayed in Fig. 2, the light output with ESR film is the highest among several reflectors, including Tyvek paper, ESR film, and Teflon tape. Therefore, we compared the light output of a CsI(Tl) crystal covered with these reflectors using an ^{241}Am source. The results are presented in Fig. 4. For each reflector, we packed the same crystal thrice, and the average light output is plotted in Fig. 4. The protective coating on each ESR film was eliminated before encapsulating the crystals. Using the ESR film with a thickness of 80 µm (red squares), the light output was larger than using Tyvek paper (blue stars), and the resolutions were nearly equivalent. The 80-µm-thick ESR film outperformed the 65-µm-thick film, probably because of its varying hardness values, which produce various reflectance effects at the edges of the crystals.

As displayed in Fig. 4a, the light output decreases as the scan point becomes more proximate to the PD or the longer side of the entrance surface, regardless of the reflector type used. This result demonstrates that the variation trend is nearly independent of the reflectors, which was consistent with the results for tapering CsI(Tl) crystals reported in Refs. [16, 28–30]. The non-uniformity in the light output (ΔLO) recorded herein is defined as [16, 29]

$$\Delta LO = \frac{C_{\max} - C_{\min}}{\frac{1}{N}\sum_{i=0}^{N} C_i} \times 100\% \tag{1}$$

where $N = 4$ denotes the number of measurement points, C_i refers to the centroid of the Gaussian peak in the energy spectra measured at different scan positions, and $C_{\max}$ and $C_{\min}$ represent the maximum and minimum values of C_i, respectively. The ΔLO values were 13.9, 16.2, and 15.5% for the 80-µm-thick, 65-µm-thick ESR films, and Tyvek paper, respectively.

In summary, the light output as well as the ΔLO value of the 80-µm-thick ESR film were superior to those of the other two reflectors. Therefore, it was selected as the final reflector for the CsI(Tl) array.

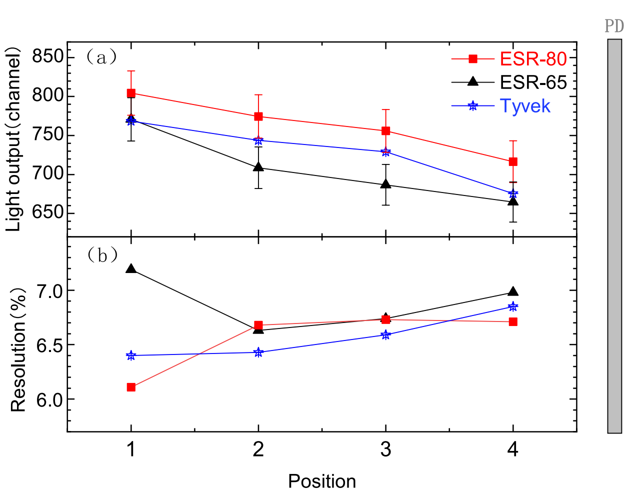

Fig. 4 (**a**) Light output and (**b**) energy resolution of a typical wedge-shaped CsI(Tl) detector wrapping with varying reflectors as a function of the scan positions. Four points along the height of the entrance surface covered by a 2-µm-thick aluminized Mylar film were measured using an ^{241}Am source. Gray rectangle denotes the PD, which is most proximate to position 4 and farthest away from position 1

3 CsI(Tl) detector arrays

Two annular arrays of 24 CsI(Tl) detectors were manufactured to match the annular DSSDs and formed two sets of $\Delta E - E$ telescopes. Images of the two arrays are depicted in Fig. 5. The light output, its variation along the height and length of each crystal, and the energy resolution were investigated for each CsI(Tl) detector using an ^{241}Am source. If the source was placed at scan position 2, the typical signal-to-noise ratio after preamplifier was 7:1 as measured using an oscilloscope.

Among the 24 crystals, Figs. 6 and 7 display various typical light output variations and the corresponding energy resolutions along the height and length, respectively. In Fig. 6a, along the height of the crystal, the decreasing (Trend1, black square), the increasing (Trend2, red point), and the nearly unchanging (Trend3, blue triangle) trend are observed for crystals from the same batch using the same reflectors (ESR film) and PDs. Among the 24 crystals, 13, 8, and 3 exhibited decreasing, increasing, and unchanging

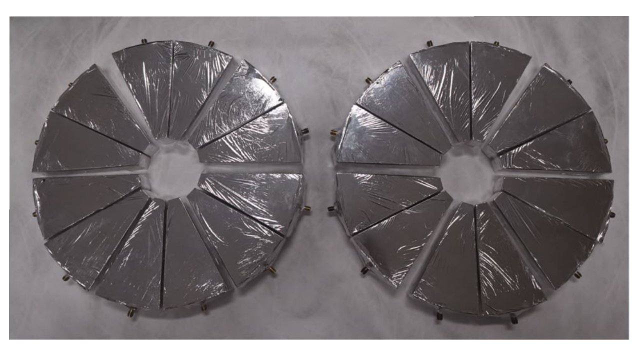

Fig. 5 Image of two annular CsI(Tl) detector arrays

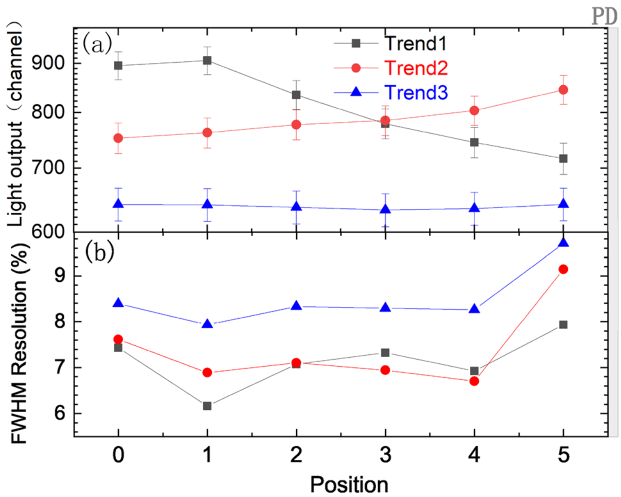

Fig. 6 Along the height of the CsI(Tl) scintillator, several typical kinds of **a** light output variation and **b** energy resolution over various scan positions. Grey rectangle represents the PDs

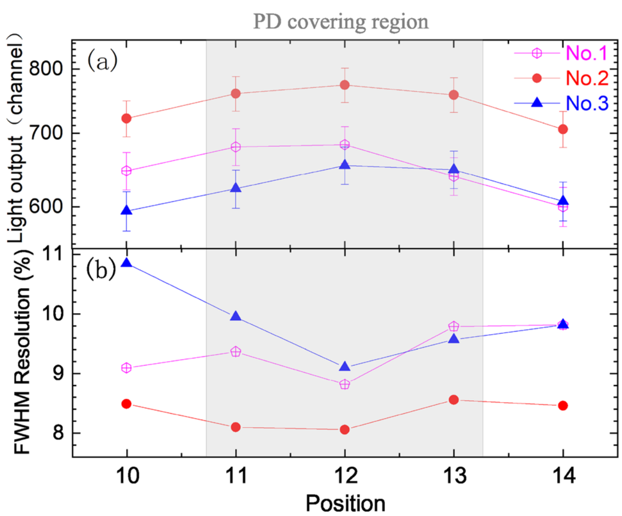

Fig. 7 Similar to Fig. 6 but along the length of the CsI(Tl) scintillator; gray rectangle represents the region covered by PDs

trends, respectively. The variation trend is independent of the reflector and PD, but relies on the intrinsic properties of the bare crystals, such as uneven Tl doping and surface roughness. Owing to their softness, the CsI(Tl) crystal surfaces can be facilely damaged during polishing, producing moderate variation in roughness, even when nominally polished. The phenomenon of light-output nonuniformity caused by uneven Tl doping has been observed in HIRA and CALIFA [7, 31, 32]. However, dopant variation along the crystals used in this study has not yet been measured. In future, these two factors should be quantitatively and carefully investigated to improve the properties of CsI(Tl) detectors. As illustrated in Fig. 6b, regardless of the type of trend, the resolution worsens at both ends of the crystals but alters slightly in the middle. The resolution decreased with the light output and the worst resolution occurred when the scan position was most proximate to the PD.

As displayed in Fig. 7a, the light output varied across multiple positions along the longer side (in the vicinity of the PD). Nonetheless, the overall trend remained consistent. The light output remained nearly constant at the scan positions in the regions covered by the PD (middle-three positions, grey region in Fig. 7), whereas it decreases rapidly in the regions uncovered by the PD (positions at both ends). If the PD size can cover the entire readout surface of the crystal, a more improved resolution can be achieved at both ends. However, this study employed the largest active area of the PD. The SiPM array can cover the entire readout surface of our CsI(Tl) crystal and has been designed to upgrade the performance of the CsI(Tl) arrays. A high-gain SiPM is beneficial for enhancing the light output and further improving the energy resolution. The variation trend of the energy resolution is similar to that observed in Fig. 6b, where the resolution deteriorated as the light output decreased.

Two-dimensional correlation histograms between the average energy resolution and either the average light output or ΔLO values along its height are summarized in Fig. 8. The energy resolution and light output were averaged using the values measured at four middle-scan positions. The results at both ends were not considered because they varied rapidly with the scan positions and were not carefully controlled. The test results for the two CsI(Tl) detectors with energy resolutions worse than 8% are not plotted in Fig. 8. As indicated by the dashed lines in Fig. 8, the

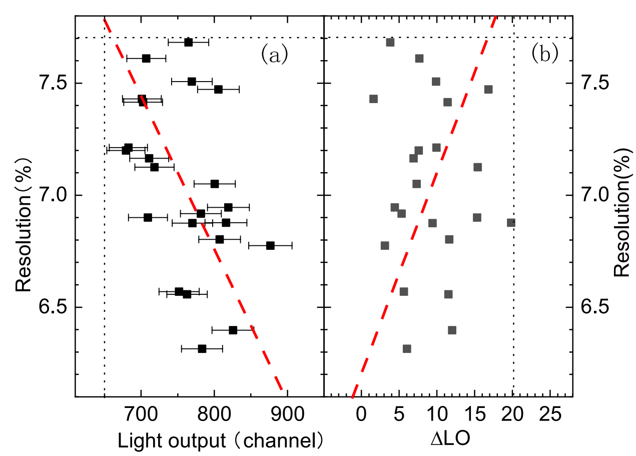

Fig. 8 Average energy resolution verse: **a** average light output and **b** ΔLO values. The average values were averaged across the values measured at scan positions along its height of the crystals. Red dashed lines aim to improve and guide visualization. Thin black dotted lines denote the final acceptance criterions for energy resolution (≤7.7%), light output (>650), and ΔLO (≤20%)

average values of the energy resolution decrease as the light output increases and increase as the ΔLO values increase.

The nonuniformity in light output can diminish the energy resolution of the CsI(Tl) detector, and eventually, affect the particle identification (PID) capability of annular telescopes. Therefore, the ΔLO value was limited to 20%. To ensure PID capability, we restricted the average energy resolution to less than $\leq$7.7% and a light output higher than 650 channels. Based on these criterions, two CsI(Tl) detectors were remanufactured.

4 Particle identification of the annular Si-CsI(Tl) telescope

Two annular Si-CsI(Tl) arrays, TA-upstream and TA-downstream, were employed for the first time in a direct nuclear reaction experiment of $^{14-16}$C + d performed at the Radioactive Beam Line in Lanzhou (RIBLL) in 2022. The experimental setup is illustrated in Fig. 1. The beam purities of $^{14-16}$C exceeded 97% with beam intensities of approximately 8.8×10^4, 3.0×10^4, and 3.3×10^4 particles per second. A CD_2 target with thickness of 9.53 mg/cm^2 was used. For the $^{14-16}$C beam, the full width at half maximum (FHWM) values of the beam spot size in the horizontal direction were 18.0, 19.0, and 20.0 mm, respectively, while they were 13.5, 16.0, and 22.0 mm in the vertical direction, respectively.

Typical PID spectra are illustrated in Figs. 9. p, d, t, ^{3}He, and ^{4}He can be prominently identified if a strip is employed as a ΔE detector, depicted in Fig. 9a. A small number of ^{3}He particles were faintly observed in Fig. 9a; however, they cannot be accurately identified as they do not form an evident band. In this case, we must sum all the strips in a DSSD as a ΔE detector to increase the statistics. However, the different thicknesses and gain deviations in the electronics of each strip, as well as the light output nonuniformity of the CsI(Tl) detector, should be carefully reviewed before summing them up. First, the DSSD is positioned perpendicular to the beam line instead of being directed in the outgoing direction of the charged particles emitted from the physical target. Therefore, the real punching through thickness of the charged particles in the DSSD is dependent on their outgoing angles. This variation can be corrected strip-by-strip using the function $d/\cos\theta$, where d denotes the nominal thickness of the DSSD (150 or 400 μm) and θ indicates the outgoing angle of a straight line defined by the center of each annular strip and the target relative to the beam line. Second, the gain deviation in the electronics can be normalized using energy calibration or the normalization method given in Ref. [33]. Third, the various trends of nonuniformity in light output of the wedge-shaped CsI(Tl) detector (Fig. 7) can be extracted and normalized using particles with preset energies such as an α source, 15-MeV protons, or 30-MeV ^{4}He particles [16]. After correcting the above three factors and completing the energy calibrations, the PID spectra of one DSSD and one CsI(Tl) detector are displayed in Fig. 9b, p, d, t, ^{3}He, and ^{4}He can be distinctly discriminated, and the ^{3}He band is more evident after adding all strips in a DSSD.

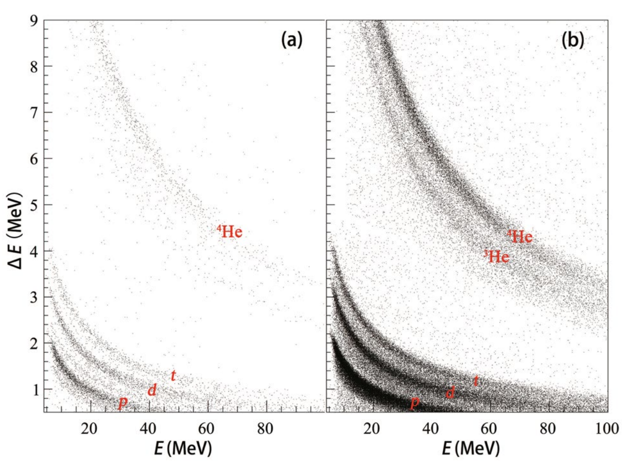

Fig. 9 Particle identification spectra of the annular Si-CsI(Tl) telescope measured in the direct nuclear reaction experiment of $^{14-16}$C + d, when using a single annular strip (**a**), a piece of DSSD after normalizing the punching through thickness strip-by-strip as a ΔE detector (**b**) and one CsI(Tl) as an E detector

5 Summary

In summary, we constructed two annular CsI(Tl) detector arrays comprising 24 wedge-shaped crystals, and tested them using an ^{241}Am source and radioactive beams. A single crystal encapsulated with various reflectors was tested. As observed, both the amount and nonuniformity of the light output were the best if an 80-μm-thick ESR film was adopted as the reflector. Therefore, all 24 wedge-shaped crystals were packed with 80-μm-thick ESR films. The energy resolution, light output, and variations in the height and length of each CsI(Tl) detector were carefully investigated. The energy resolution improved and deteriorated as the light output and ΔLO value increased, respectively. For the first time, two annular Si-CsI(Tl) telescopes were tested in a direct nuclear reaction experiment using $^{14-16}$C + d. The $Z = 1$ and $Z = 2$ charged particles were sufficiently discriminated using the entire DSSD as a single ΔE detector. In the future, we should enhance the light output and reduce the ΔLO value of the wedge-shaped CsI(Tl) detector as much as possible to further improve the PID capability. For instance, this can be achieved by adopting SiPMs with larger active areas and higher gains as photon detection devices and improving the intrinsic properties of the CsI(Tl) crystal.

Author Contributions All authors contributed to the study conception and design. Material preparation, data collection and analysis were performed by Hong-Yu Zhu, Jian-Ling Lou and Bo-Long Xia. The first draft of the manuscript was written by Jian-Ling Lou and all authors commented on previous versions of the manuscript. All authors read and approved the final manuscript.

Data Availability The data that support the findings of this study are openly available in Science Data Bank at https://www.doi.org/10.57760/sciencedb.j00186.00253 and https://cstr.cn/31253.11.

Declarations

Conflict of interest The authors declare that they have no competing interests.

References

1. B. Davin, R.T. de Souza, R. Yanez et al., LASSA: a large area silicon strip array for isotopic identification of charged particles. Nucl. Instrum. Methods Phys. Res. A **473**, 302 (2001). https://doi.org/10.1016/S0168-9002(01)00295-9
2. E. Pollacco, D. Beaumel, P. Roussel-Chomza et al., MUST2: A new generation array for direct reaction studies. Eur. Phys. J. A **25**, 287 (2005). https://doi.org/10.1140/epjad/i2005-06-162-5
3. L. Acosta, E.V. Pagano, T. Minniti et al., FARCOS, a new array for femtoscopy and correlation spectroscopy. EPJ Web. Conf. **31**, 00035 (2012). https://doi.org/10.1051/epjconf/20123100035
4. L. Acosta, R. Andolina, L. Auditore et al., Campaign of measurements to probe the good performance of the new array FARCOS for spectroscopy and correlations. J. Phys. Conf. Ser. **730**, 012001 (2016). https://doi.org/10.1088/1742-6596/730/1/012001
5. M.S. Wallace, M.A. Famiano, M.-J. van Goethem et al., The high resolution array (HiRA) for rare isotope beam experiments. Nucl. Instrum. Methods Phys. Res. A **583**, 302 (2007). https://doi.org/10.1016/j.nima.2007.08.248
6. D. Dell'Aquila, I. Lombardo, G. Verde et al., OSCAR: A new modular device for the identification and correlation of low energy particles. Nucl. Instrum. Methods Phys. Res. A **877**, 227–237 (2018). https://doi.org/10.1016/j.nima.2017.09.046
7. D. Dell'Aquila, S. Sweany, K.W. Brown et al., Non-linearity effects on the light-output calibration of light charged particles in CsI(Tl) scintillator crystals. Nucl. Instr. Meth. A **929**, 162–172 (2019). https://doi.org/10.1016/j.nima.2019.03.065
8. W. Liu, J.L. Lou, Y.L. Ye et al., Experimental study of intruder components in light neutron-rich nuclei via a single nucleon transfer reaction. Nucl. Sci. Tech. **31**, 20 (2020). https://doi.org/10.1007/s41365-020-0731-y
9. G. Li, Z.W. Tan, J.L. Lou et al., Study on exotic structure of light neutron-rich nuclei via direct reaction. Nucl. Phys. Rev. **37**, 426–437 (2020). https://doi.org/10.11804/NuclPhysRev.37.2019CNPC09. (**in Chinese**)
10. J.L. Lou, Y.L. Ye, Z.H. Yang et al., Progress of exotic structure studies in light neutron-rich nuclei. Chin. Sci. Bull. **68**, 1004–1015 (2023). https://doi.org/10.1360/TB-2022-0942
11. J. Chen, J.L. Lou, Y.L. Ye et al., Low-lying states in ^{12}Be using one-neutron transfer reaction. Phys. Rev. C **98**, 014616 (2018). https://doi.org/10.1103/PhysRevC.98.014616
12. J. Chen, J.L. Lou, Y.L. Ye et al., A new measurement of the intruder configuration in ^{12}Be. Phys. Lett. B **781**, 412–416 (2018). https://doi.org/10.1016/j.physletb.2018.04.016
13. J. Chen, J.L. Lou, Y.L. Ye et al., Observation of the near-threshold intruder 0^- resonance in ^{12}Be. Phys. Rev. C **103**, L031302 (2021). https://doi.org/10.1103/PhysRevC.103.L031302
14. Y. Liu, Y.L. Ye, J.L. Lou et al., Positive-parity linear-chain molecular band in ^{16}C. Phys. Rev. Lett. **124**, 192501 (2020). https://doi.org/10.1103/PhysRevLett.124.192501
15. Y. Jiang, J.L. Lou, Y.L. Ye et al., Quadrupole deformation of ^{16}C studied by proton and deuteron inelastic scattering. Phys. Rev. C **101**, 024601 (2020). https://doi.org/10.1103/PhysRevC.101.024601
16. G. Li, J.L. Lou, Y.L. Ye et al., Property investigation of the wedge-shaped CsI(Tl) crystals for a charged-particle telescopes. Nucl. Instr. Meth. A **1013**, 165637 (2021). https://doi.org/10.1016/j.nima.2021.165637
17. W. Liu, J.L. Lou, Y.L. Ye et al., s- and d-wave intruder strengths in $^{13}B_{g.s.}$ via the ^{1}H(^{13}B, d)^{12}B reaction. Phys. Rev. C **104**, 064605 (2021). https://doi.org/10.1103/PhysRevC.104.064605
18. W. Liu, J.L. Lou, Y.L. Ye et al., New investigation of low-lying states in ^{12}Be via a ^{2}H(^{13}B, ^{3}He) reaction. Phys. Rev. C **105**, 034613 (2022). https://doi.org/10.1103/PhysRevC.105.034613
19. Z.W. Tan, J.L. Lou, Y.L. Ye et al., Investigation of negative-parity states in ^{16}C via deuteron inelastic scatter. Chin. Phys. C **46**, 054001 (2022). https://doi.org/10.1088/1674-1137/ac488b
20. J.X. Han, Y. Liu, Y.L. Ye et al., Observation of the $\Pi^2\sigma^2$-bond linear-chain molecular structure in ^{16}C. Phys. Rev. C **105**, 044302 (2022). https://doi.org/10.1103/PhysRevC.105.044302
21. Y. Sun, Z.Y. Sun, Y.H. Yu et al., Temperature dependence of CsI: Tl coupled to a PIN photodiode and silicon photomultiplier. Nucl. Sci. Tech. **30**, 27 (2019). https://doi.org/10.1007/s41365-019-0551-0
22. Hamamatsu Photonics S3584-08, www.hamamatsu.com/jp/en/product/type/S3584-08/index.html
23. ORTEC 572A amplifier Manual. https://www.ortec-online.com.cn/products/electronics/amplifiers/572a
24. L.Y. Ma, H. Hua, F. Lu et al., A CsI(T1) detector array used in the experiment of Proton-rich nucleus ^{17}Ne. Chin. Phys. C (SupplB) **33**, 176–178 (2009). https://doi.org/10.1088/1674-1137/33/S1/056
25. Enhanced Specular Reflector Films, https://www.3m.com software
26. M. Janecek, W.W. Moses, Optical reflectance measurements for commonly used reflectors. IEEE Trans. Nucl. Sci. **55**, 2432–2437 (2008). https://doi.org/10.1109/TNS.2008.2001408
27. M. Janecek, W.W. Moses, Simulating scintillator light collection using measured optical reflectance. IEEE Trans. Nucl. Sci. **57**, 964–970 (2010). https://doi.org/10.1109/TNS.2010.2042731
28. J. Bea, A. Gadea, L.M. Garcia-Raffi et al., Simulation of light collection in scintillators with rough surfaces. Nucl. Instrum. Methods Phys. Res. A **350**, 184–191 (1994). https://doi.org/10.1016/0168-9002(94)91162-2
29. A. Knyazev, J. Park, P. Golubev et al., Properties of the CsI (Tl) detector elements of the CALIFA detector. Nucl. Instrum. Methods Phys. Res. A **940**, 393–404 (2019). https://doi.org/10.1016/j.nima.2019.06.045
30. E. Auffray, F. Cavallari, M. Lebeau et al., Crystal conditioning for high-energy physics detectors. Nucl. Instrum. Methods Phys. Res. A **486**, 22–34 (2002). https://doi.org/10.1016/S0168-9002(02)00670-8
31. A. Knyazev, J. Park, P. Golubev et al., Tl concentration and its variation in a CsI(Tl) crystal for the CALIFA detector. Nucl. Instrum. Methods Phys. Res. A **975**, 164197 (2020). https://doi.org/10.1016/j.nima.2020.164197
32. Q. Liu, Y.L. Ye, Z.H. Li et al., Investigation of the thickness non-uniformity of very thin silicon strip etectors. Nucl. Instrum. Methods Phys. Res. A **897**, 100–105 (2018). https://doi.org/10.1016/j.nima.2018.100

33. R. Qiao, Y.L. Ye, J. Wang et al., A new uniform calibration method for double-sided silicon strip detectors. IEEE T. Nucl. Sci. **61**, 596–601 (2014). https://doi.org/10.1109/TNS.2013.2295519